

# Atmospheric glories: simulations and observations

Philip Laven

Mie theory can be used to provide full-color simulations of atmospheric glories. Comparison of such simulations with images of real glories suggests that most glories are caused by spherical water droplets with radii between 4 and 25  $\mu\text{m}$ . This paper also examines the appearance of glories taking into account the size of the droplets and the width of the droplet size distributions. Simulations of glories viewed through a linear polarizer compare well with the few available pictures, but they show some features that need corroboration by more observations. © 2005 Optical Society of America

OCIS codes: 010.1290, 290.4020.

## 1. Introduction

When your shadow falls on fog or clouds, you may be lucky enough to see a glory in the form of concentric colored circles surrounding the shadow of your head. Glories are caused by the backscattering of sunlight from small droplets of water. This paper uses Mie-theory calculations to examine various aspects of glories, including how their appearance varies with (a) the use of a polarizer, (b) the width of the size distribution of the water droplets, and (c) the median radius of the water droplets. It also compares simulations with some observations of real glories.

All of the graphs and simulations in this paper have been generated using the MiePlot computer program developed by the author. This program can be downloaded free of charge from <http://www.philiplaven.com/mieplot.htm>.

## 2. Mie-Theory Calculations

Mie theory<sup>1</sup> can be used to generate full-color simulations of atmospheric glories.<sup>2,3</sup> Figure 1 shows the results of Mie-theory calculations of intensity as a function of scattering angle  $\theta$  for scattering of plane-wave monochromatic red light ( $\lambda = 650 \text{ nm}$ ) from a spherical water droplet with radius  $r = 10 \mu\text{m}$ . When the polarization is perpendicular to the scattering plane, there is a strong maximum at  $178.5^\circ$ . When the polarization is parallel to the scattering plane, there are maxima at  $176.1^\circ$  and  $178.1^\circ$ .

Figure 2 shows Mie-theory results for the scattering of sunlight. In this paper, the term "sunlight" implies calculations based on a light source with an apparent angular diameter of  $0.5^\circ$  and with the spectrum of sunlight between 380 nm and 700 nm as recorded at ground level by Lee.<sup>4</sup> Note that the parallel-polarized component has its maximum intensity at  $\theta \approx 178.6^\circ$ , whereas perpendicular polarization has its maximum at  $180^\circ$ . The three horizontal bars above the graph in Fig. 2 represent the brightness and color of the scattered light for perpendicular polarization, for parallel polarization, and for unpolarized light. The red areas around  $\theta = 177.6^\circ$  and  $176.2^\circ$  correspond to the red rings of the glory, which do not coincide with the maxima shown in Fig. 1 for red light. The horizontal bar for unpolarized light has been replotted in Fig. 3(a) to simulate the appearance of a glory centered on the antisolar point  $\theta = 180^\circ$ .

## 3. Effects of Polarization

Figure 3(b) shows the appearance of the glory in Fig. 3(a) when viewed through a linear polarizer with its transmission axis vertical (equivalent to the view seen through polarized sunglasses worn in the usual orientation). The distinctive dark spots immediately above and below the antisolar point in Fig. 3(b) were predicted by Können<sup>5</sup> in his gray-scale diagram reproduced as Fig. 4. Können's diagram also suggests that the polarizer will suppress the rings of the glory to the left and right of the antisolar point. However, the rings seem to be continuous in Fig. 3(b), although the polarizer darkens the rings in these areas. Examination of Fig. 2 indicates that parallel polarization is dominant for the rings of the glory. The component due to perpendicular polarization is significantly weaker, but its colors are similar to the

Philip Laven ([philip@philiplaven.com](mailto:philip@philiplaven.com)) can be contacted at Chemin de l'Avanchet 20, CH-1216 Cointrin, Switzerland.

Received 3 January 2005; revised manuscript received 2 May 2005; accepted 3 May 2005.

0003-6935/05/275667-08\$15.00/0

© 2005 Optical Society of America

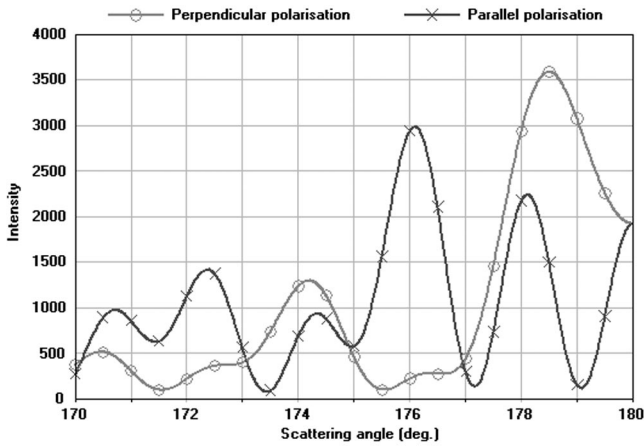
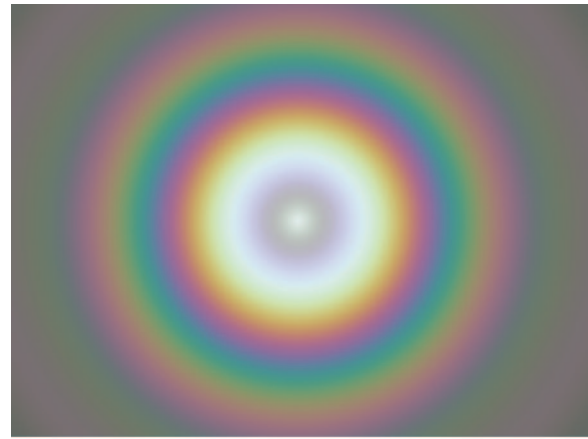


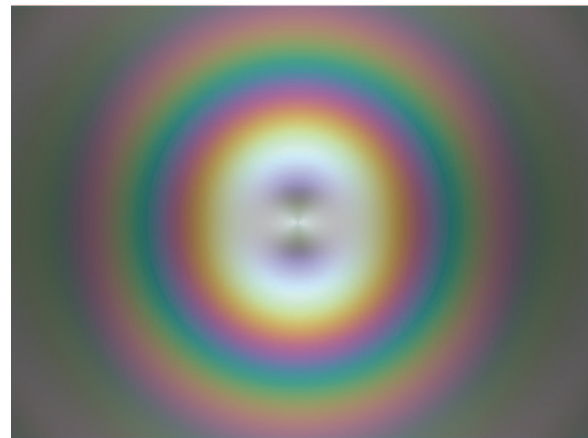
Fig. 1. Backscattering of monochromatic red light ( $\lambda = 650 \text{ nm}$ ) by a spherical water droplet with radius  $r = 10 \mu\text{m}$  as a function of scattering angle  $\theta$ . Note that “perpendicular polarization” indicates light with polarization perpendicular to the scattering plane, whereas “parallel polarization” indicates polarization parallel to the scattering plane.

parallel-polarized component. Nevertheless, careful examination reveals that the circular rings in Fig. 3(a) have become slightly elliptical in Fig. 3(b), with their width being slightly less than their height. Figure 5 shows how the use of a polarizer can produce the peculiar pattern shown in Fig. 3(b).

Glories are frequently observed from commercial aircraft where it is difficult to observe subtle polarization effects because stresses in aircraft windows change the state of polarization.<sup>6</sup> Alistair Fraser’s photograph, shown in Fig. 6(a), is one of the few previously published pictures of a polarized glory.<sup>5</sup> As this paper was being finalized, the author observed a glory from an aircraft and used a vertical polarizer to capture the images shown in Figs. 6(b) and 6(c). Al-



(a)



(b)

Fig. 3. (a) Simulation of a glory caused by scattering of sunlight from spherical water droplets with  $r = 10 \mu\text{m}$  (the width of the image is about  $\pm 5^\circ$ ). (b) As in (a) but viewed through a polarizer with its transmission axis vertical.

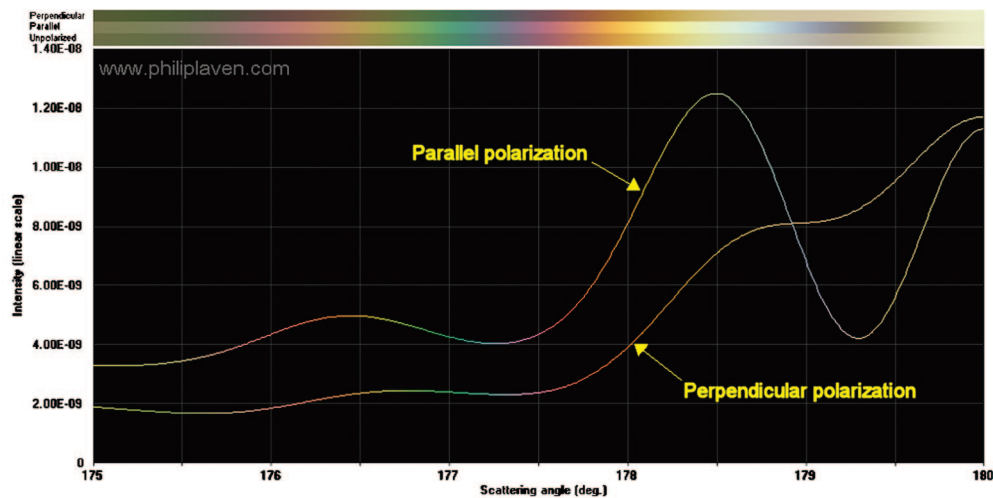


Fig. 2. Backscattering of sunlight from a spherical droplet of water with  $r = 10 \mu\text{m}$  as a function of scattering angle  $\theta$ . These calculations were based on a light source with an apparent angular diameter of  $0.5^\circ$  with the spectrum of sunlight represented by 300 discrete wavelengths between 380 nm and 700 nm. The three horizontal colored bars above the graph represent the brightness and color of the scattered light for perpendicular polarization, parallel polarization, and unpolarized light, while the color of the curves in the graph shows the saturated color of the scattered light.

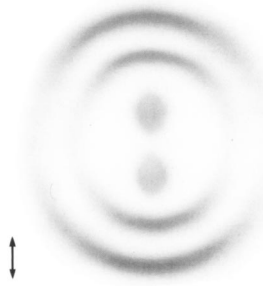


Fig. 4. Diagram showing the appearance of a glory when viewed through a polarizer with its transmission axis vertical. Reproduced with permission of G. P. Können.

though the camera was held in the same nominal position, the axis of polarization in Fig. 6(b) appears to be tilted by 20 degrees anticlockwise from its expected orientation, while in Fig. 6(c) it is tilted by about 70 degrees clockwise. The orientation appears to be dependent on which part of the aircraft window the camera was looking through. There is obviously a need for further images of glories recorded through polarizers, especially those taken by mountaineers or balloonists who can see glories without having to look through windows! In response to my personal request, Claudia Hinz has kindly taken several such pictures of polarized glories, one of which is shown in Fig. 6(d), where a dark spot is clearly visible directly above the antisolar point. All of the photographs in Fig. 6 show the predicted dark spots, but they do not completely resolve whether the colored rings are continuous or slightly elliptical.

#### 4. Size Distribution of Droplets

The above simulations assume that all of the water droplets are exactly the same size (i.e., monodisperse). In real fog or clouds, this assumption is not valid. Simulations of scattering from disperse droplets are shown in Figs. 7(a)–7(c); these are based on Mie-theory calculations for 50 values of radius  $r$  having a log-normal distribution with a median value of  $10 \mu\text{m}$  and the specified standard deviation  $\sigma$ . Comparison of Figs. 7(a)–7(c) with the monodisperse result in Fig. 3(a) shows that the outer rings become progressively fainter as  $\sigma$  increases. When  $\sigma$  is 5% of the median value of  $r$ , the colored rings are only slightly less saturated than for the monodisperse case. However, when  $\sigma = 20\%$ , the colored rings of the glory are not visible, apart from a faint white ring tinged with red on its outer edge.

Lenticular clouds seem to produce especially vivid glories with multiple rings. Various authors<sup>7–9</sup> have reported that such clouds often produce brightly colored coronas and have postulated that this is because the water droplets in such clouds have a very narrow distribution of sizes.

Examination of images of vivid natural glories implies that, in many cases,  $\sigma < 5\%$ . Mayer<sup>10</sup> reported measurements of a glory indicating that the clouds causing the glory had an effective radius of about  $11 \mu\text{m}$  with  $\sigma \approx 1 \mu\text{m}$  (9%). Both of these results suggest a much narrower size distribution than the widely used C1 gamma distribution proposed by Deirmendjian<sup>11</sup> for cumulus clouds. In practice, cumulus clouds rarely produce vivid glories, presum-

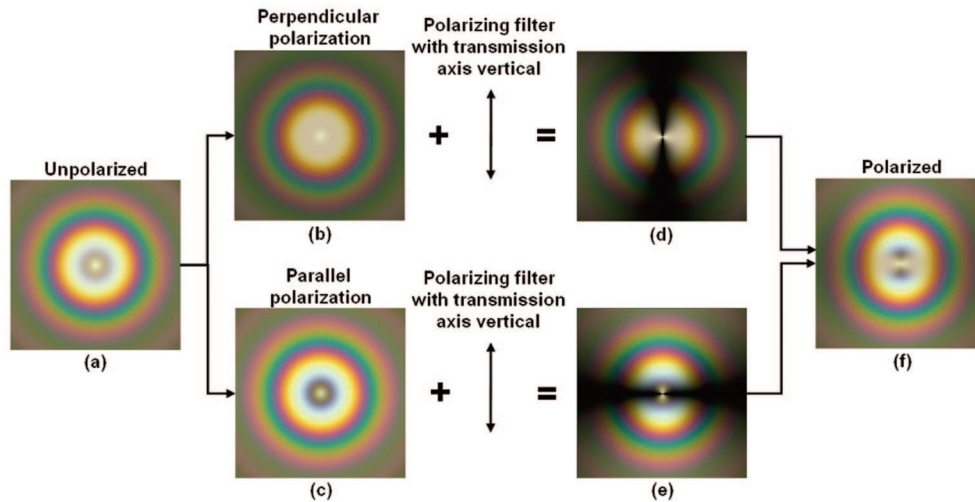


Fig. 5. An unpolarized glory, shown as image (a), can be separated into two components (b) and (c), which have polarizations perpendicular and parallel to the scattering plane, respectively. When viewed through a vertical polarizer, (b) is transformed into (d), while (c) is transformed into (e). Image (d) shows that the polarizer suppresses perpendicular polarization along the vertical line through the antisolar point, but has no effect along the horizontal line. This is similar to the effect of viewing the primary rainbow through a polarizer, because the primary rainbow is dominated by perpendicular polarization. Image (e) shows that the polarizer suppresses parallel polarization along the horizontal line through the antisolar point. When (d) and (e) are combined, the resulting image (f) shows the “polarized” glory with its distinctive dark spots above and below the antisolar point. Note that the colors of the polarized glory along the horizontal line through the antisolar point correspond to perpendicular polarization, whereas those along the vertical correspond to parallel polarization. Other orientations obviously involve a mixture of the two polarizations.



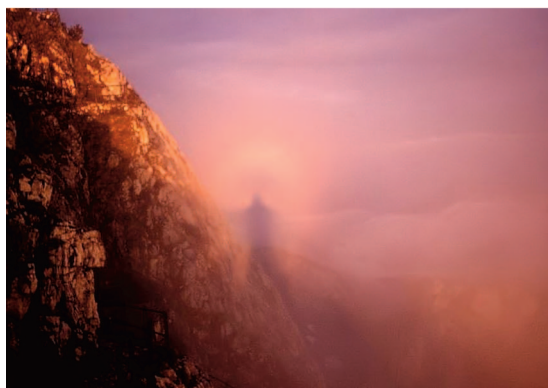
(a)



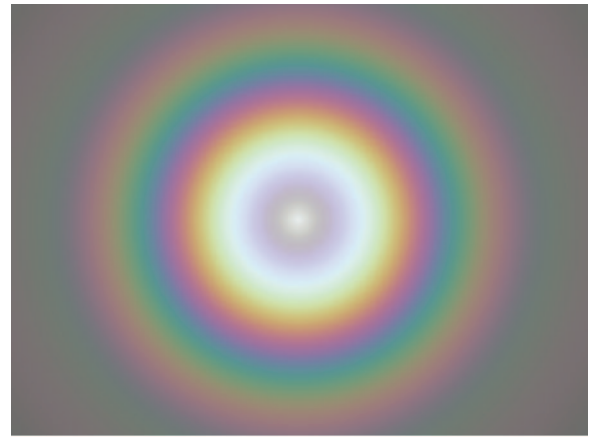
(b)



(c)



(d)



(a)



(b)



(c)

Fig. 7. Simulations of glories caused by water droplets with a log-normal size distribution with median value of  $r = 10 \mu\text{m}$  and standard deviation  $\sigma$ : (a)  $\sigma = 0.5 \mu\text{m}$ , (b)  $\sigma = 1 \mu\text{m}$ , (c)  $\sigma = 2 \mu\text{m}$ .

Fig. 6. Photographs of glories viewed through a polarizer with the transmission axis vertical. Reproduced with permission of: (a) Alistair Fraser, (b) Philip Laven, (c) Philip Laven, (d) Claudia Hinz.

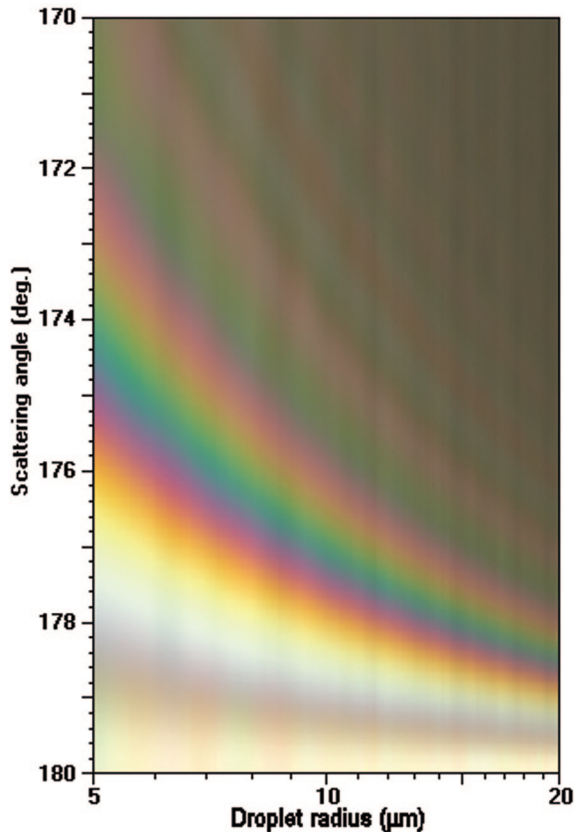


Fig. 8. Scattering of sunlight by water droplets of median radius  $r$  between 5  $\mu\text{m}$  and 20  $\mu\text{m}$  with a log-normal size distribution and a standard deviation  $\sigma = 5\%$  of the nominal value.

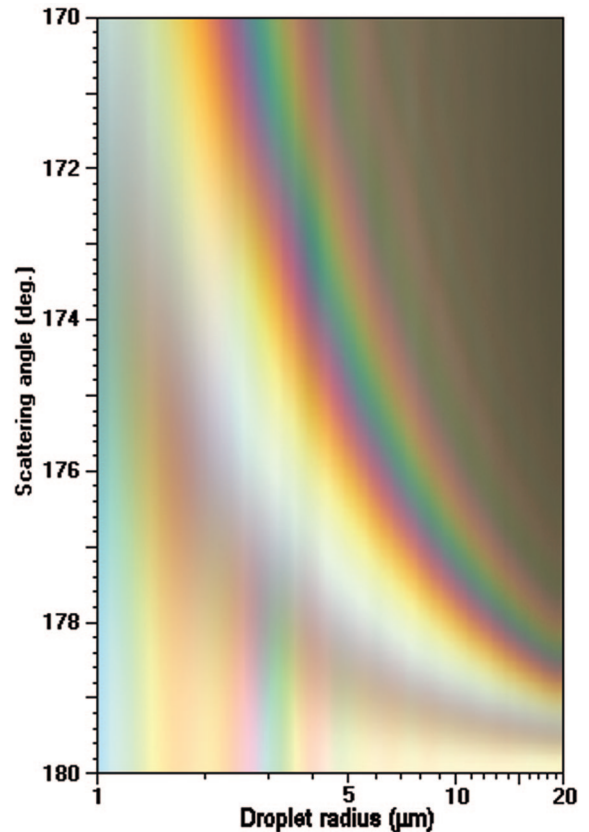


Fig. 9. Scattering of sunlight by water droplets of median radius  $r$  between 1  $\mu\text{m}$  and 20  $\mu\text{m}$  with a log-normal size distribution and a standard deviation  $\sigma = 5\%$  of the nominal value.

ably because such clouds contain water droplets with a wide size distribution.

### 5. Droplet Size

The size of the water droplets can be inferred from the angular size of the rings in a glory. Large rings imply small droplets, while small rings imply large droplets, as illustrated in Fig. 8. To a first approximation, the radius of the rings is inversely proportional to the radius  $r$  of the water droplets: the four inner red rings appear at radii (measured in degrees) of approximately  $24/r$ ,  $37/r$ ,  $56/r$ , and  $76/r$  (where  $r$  is measured in  $\mu\text{m}$ ). For example, for  $r = 10 \mu\text{m}$ , the innermost red ring appears at a radius of about  $2.4^\circ$  from the antisolar point, which corresponds to  $\theta = 177.6^\circ$ .

Note that the sequence of colors shown in Fig. 8 is essentially independent of  $r$ . However, when the range of  $r$  is expanded down to 1  $\mu\text{m}$ , as in Fig. 9, the pattern of colors becomes much more complicated. The vertical bands of color in the lower left part of Fig. 9 imply that the central feature of the glory should have distinct colors for  $r < 4 \mu\text{m}$ . As  $r$  is reduced below 4  $\mu\text{m}$ , the center of the glory changes from red to orange, yellow, green, blue, and violet until  $r \approx 2.7 \mu\text{m}$ , when this color sequence starts to repeat itself. To the author's knowledge, glories with colored centers have not been reported.

Comparisons of images of real glories with simulations suggests that most glories are caused by scattering from water droplets with  $r$  between about 4  $\mu\text{m}$  and 25  $\mu\text{m}$ . The upper limit may be a consequence of the increased path length traversed by the surface waves that are responsible for formation of the glory.<sup>12</sup> Another reason for the upper limit is that large droplets produce small glories in which the fine details are smeared by the Sun's apparent angular diameter of  $0.5^\circ$ . Figure 10 compares the glory for  $r = 30 \mu\text{m}$  generated by a point source and by a  $0.5^\circ$  light source. The reason for the lower limit of about 4  $\mu\text{m}$  is more difficult to explain, especially as some of the best glories seen by the author correspond to  $4 \mu\text{m} < r < 5 \mu\text{m}$ . This apparent lower limit may be due to the reduced intensity of glories caused by scattering from very small droplets or due to the rarity of such water droplets in the atmosphere.

### 6. Observations of Glories

This section compares Mie-theory simulations with images of real glories. An immediate problem is that most people taking photographs of glories do not know the focal length of the camera lens, especially if it is a zoom lens. This is becoming less of a problem because digital cameras record the camera's settings with the image. Furthermore, as the nominal focal length quoted by the manufacturer is often inaccu-

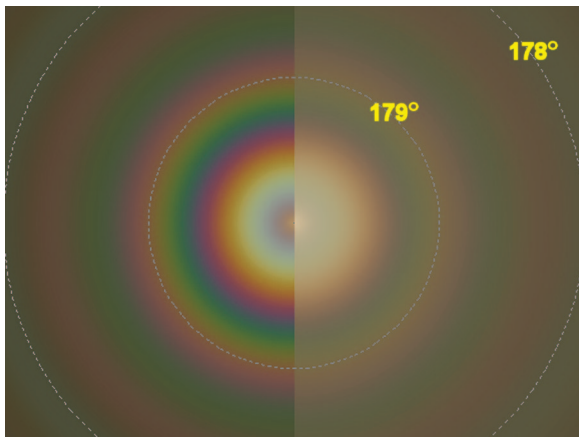


Fig. 10. Simulation of the glory due to scattering by  $r = 30 \mu\text{m}$  droplets of water: the left side shows the glory caused by a point source of light, while the right side shows the glory caused by a light source with an apparent diameter of  $0.5^\circ$ .

rate, careful calibration of the lens is required to understand the distortions introduced by the lens. Despite these obstacles, it is possible to demonstrate good correlation between simulations and images of glories.

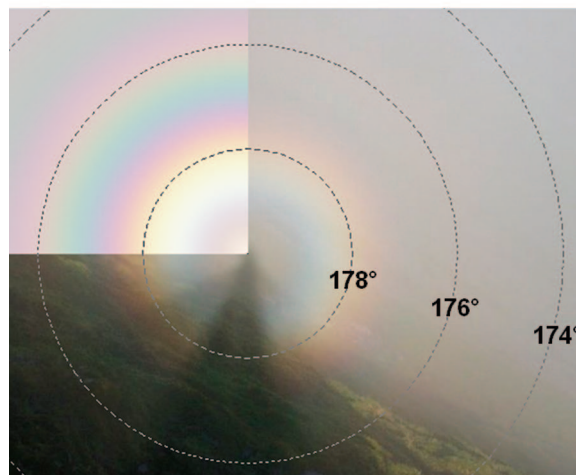
Figures 11(a) and 12(a) show magnificent images of glories as seen by mountaineers. In both cases, the glory is accompanied by the Brocken specter consisting of elongated shadows pointing toward the antisolar point. If you do see a glory, you may be perplexed by the fact that the colored rings appear only around the shadow of your own head, and not around the shadows of your companions. This effect is clearly shown in Fig. 12(a), where the rings of the glory are centered on the shadow of the photographer's head, while the shadow of the mountaineer in the yellow jacket is not "blessed" by such rings. Of course, your companions see rings around their own shadows, but not around yours. Even more strangely, if you take a picture with a camera at the end of your outstretched arm, the picture will show rings around the shadow of the camera.

Glories usually appear against a nearly white background caused by multiple scattering by water droplets in clouds or fog. As the simulations shown in the earlier part of this paper ignore the effects of multiple scattering, they do not have a white background. When comparing simulations with images of natural glories, it is necessary to address this deficiency. In the following simulations, a uniform background color has simply been added to each of the simulations with the objective of matching the background color seen on the corresponding image. Further work is planned to include the effects of multiple scattering in MiePlot simulations.

Figure 11(b) shows a simulation of a glory caused by the scattering of sunlight by water droplets with radius  $r = 9 \mu\text{m}$  superimposed on the image seen in Fig. 11(a). An unusual feature of the glory in Fig. 11(a) is that the inner ring appears to be orange, rather than red as predicted by the simulation. Sim-



(a)



(b)

Fig. 11. (a) Glory and a Brocken specter seen in Grisedale, Cumbria, England (image reproduced with permission of Dave Newton). (b) Simulation of a glory caused by monodisperse water droplets with  $r = 9 \mu\text{m}$ .

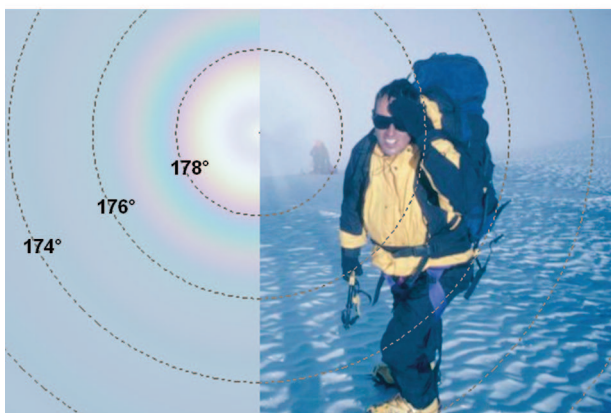
ilarly, Fig. 12(b) shows a simulation for  $r = 11 \mu\text{m}$  superimposed on Fig. 12(a).

Until the advent of air travel, glories were seen only by mountaineers. Nowadays, observant air travelers have many opportunities to see atmospheric glories: for example, the author has taken more than 2000 digital pictures of glories while traveling on commercial aircraft in the past 5 years. Figure 13(a) shows a glory observed shortly after an aircraft climbed through the cloud layer, while Fig. 13(b) shows a simulation of a glory for  $r = 4.3 \mu\text{m}$ .

Figure 14 shows an image of an unusual glory. It was recorded on 28 January 2003 by the MEIDEX (Mediterranean Israeli Dust Experiment) instrument on board the space shuttle Columbia, which tragically burnt up on re-entry into the Earth's atmosphere on 1 February 2003, resulting in the deaths of all seven members of the crew. The MEIDEX Science Team at Tel Aviv University found this fascinating image while examining the results of



(a)

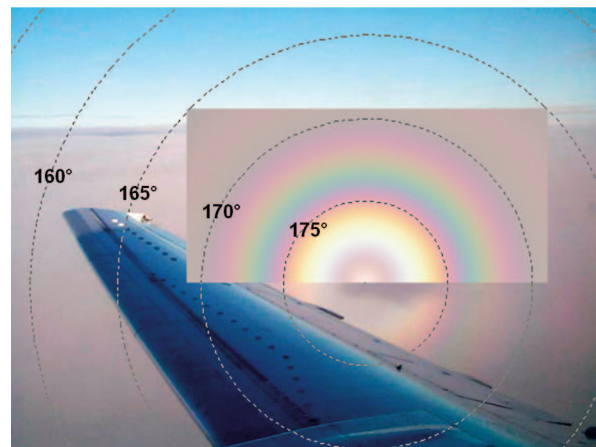


(b)

Fig. 12. (a) Glory and a Brocken specter seen very close to the summit (22 600 ft; 6888 m) of Mt. Aconcagua, Argentina (picture taken by Eric Wintenberger and reproduced with permission of Pedro Gonzalez). (b) Simulation of a glory caused by monodisperse water droplets with  $r = 11 \mu\text{m}$ .



(a)



(b)

Fig. 13. (a) Glory seen from a commercial aircraft (Philip Laven). (b) Simulation of a glory caused by monodisperse water droplets with  $r = 4.3 \mu\text{m}$ .

MEIDEX and have suggested that the term “Astronaut’s glory” should be used “in honor of our friends from the Columbia crew.” The inset in Fig. 14 compares the observed glory with a MiePlot simulation assuming water droplets with radius  $r = 16 \mu\text{m}$ . As the slant distance from the space shuttle to the antisolar point on the cloud layer was about 310 km, the red ring of the glory has a diameter (on the clouds) of approximately 16 km.

Despite the generally good agreement between observations and simulations reported above, many observers report that cameras (film or digital) do not seem to capture the brilliance of glories observed directly by human eyes. For example, glories with five red rings are occasionally observed, yet images of these glories typically show only the innermost two or three red rings with very feeble outer rings. Image processing can enhance the visibility of the outer rings, but it is relevant to note that, even in simulations under ideal conditions, the fourth and fifth rings are barely visible. Furthermore, simulations often show bright green rings, whereas observations and photographs rarely show more than a hint of green.

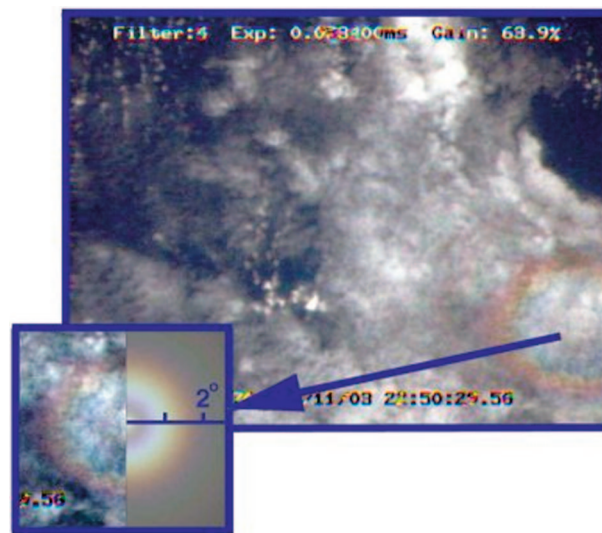


Fig. 14. Glory observed by the MEIDEX instrument on board the Space Shuttle Columbia (image reproduced with permission of Peter Israelevich, Tel Aviv University).

As noted in an earlier paper,<sup>3</sup> such problems reinforce the need for further work to define the colors corresponding to specific wavelengths of light in terms of red-green-blue values used within computers, as well as to take account of the characteristics of the display devices, such as computer screens, projectors, or printers.

## 7. Conclusions

Mie theory can be used to generate reasonably good full-color simulations of glories. Comparisons with images of natural glories indicate that most glories are caused by water droplets with radius  $r$  between about 4  $\mu\text{m}$  and 25  $\mu\text{m}$ . The most vivid glories seem to be caused by water droplets with a very narrow size distribution, such as a log-normal distribution with standard deviation of less than 5% of the median radius.

The simulations also reveal some features of glories that deserve further corroboration by observations, such as the appearance of glories when viewed through a polarizer and the appearance of glories caused by water droplets with radius  $r < 4 \mu\text{m}$ .

## References

1. G. Mie, "Beitrage zur Optik trüber Medien, speziell kolloidaler Metallosungen," *Ann. Phys. Leipzig* **25**, 377–445 (1908).
2. S. D. Gedzelman, "Simulating glories and cloudbows in color," *Appl. Opt.* **42**, 429–435 (2003).
3. P. Laven, "Simulation of rainbows, coronas, and glories by use of Mie theory," *Appl. Opt.* **42**, 436–444 (2003).
4. R. L. Lee, Jr., "Mie theory, Airy theory, and the natural rainbow," *Appl. Opt.* **37**, 1506–1519 (1998).
5. G. P. Können, *Polarized Light in Nature* (Cambridge University, Cambridge, UK, 1985).
6. C. F. Bohren, "On the gamut of colors seen through birefringent airplane windows," *Appl. Opt.* **30**, 3474–3478 (1991).
7. D. K. Lynch and W. Livingston, *Color and Light in Nature* (Cambridge University, Cambridge, UK, 2001).
8. S. D. Gedzelman and J. A. Lock, "Simulating coronas in color," *Appl. Opt.* **42**, 497–504 (2003).
9. J. A. Shaw and P. J. Neiman, "Coronas and iridescence in mountain wave clouds," *Appl. Opt.* **42**, 476–485 (2003).
10. B. Mayer, M. Schröder, R. Preusker, and L. Schüller, "Remote sensing of water cloud droplet size distributions using the backscatter glory: a case study," *Atmos. Chem. Phys.* **4**, 1255–1263 (2004).
11. D. Deirmendjian, *Electromagnetic Scattering on Spherical Polydispersions* (Elsevier, New York, 1969).
12. P. Laven, "How are glories formed?" *Appl. Opt.* **44**, 5675–5683 (2005).